Reproductive mechanism of Gram-negative protocells

Authors

Dheeraj Kanaparthi[1,2,3*], Marko Lampe[4], Jan-Hagen Krohn[1,3], Baoli Zhu[2&5], Andreas Klingl[6], & Tillmann Lueders[2*]

Affiliations

[1]Max-Planck Institute for Biochemistry, Munich, Germany.

[2]Chair of Ecological Microbiology, BayCeer, University of Bayreuth, Germany.

[3]Excellence Cluster ORIGINS, Garching, Germany.

[4]Advanced Light Microscopy Facility, European Molecular Biology Laboratory, Heidelberg, Germany.

[5]Key Laboratory of Agro-ecological Processes in Subtropical Regions, CAS, Changsha, China.

[6]Department of Biology, LMU, Planegg-Martinsried, Germany.

*Corresponding authors

Abstract

Protocells were thought to have existed on the early Earth, prior to the origin of prokaryotes. These organisms were thought to have been devoid of complex molecular biological processes and were dependent on environmental conditions for mediating reproduction. Despite these theoretical propositions, a method of cell replication mediated entirely by physicochemical properties of cell constituents has never been experimentally demonstrated. To understand the reproduction in protocells, here we used a top-down approach to transform a Gram-negative bacterium into a sack of cytoplasm devoid of all mechanisms regulating its morphology and reproduction. We then grew these cells under the environmental conditions of early Earth. Despite the loss of molecular biological coordination, cells in our study reproduced in a defined sequence of steps. The reproductive process of these cells can be explained by an interplay between intracellular metabolism, physicochemical properties of cell constituents and environmental conditions. Based on our results we propose that reproduction is an inherent property of cells with intracellular metabolism. Under favorable environmental conditions, especially the ones prevalent on early Earth, should have facilitated efficient reproduction of protocells. In short, our study demonstrates how protocells reproduced prior to the evolution of molecular biological processes.

Introduction

Life on Earth is thought to have emerged in a series of steps described by the theory of chemical evolution[1]. According to this theory, organic compounds required for building a cell were synthesized by Miller-Urey[2]-like processes and subsequent prebiotic chemical reactions[3–5]. These organic compounds were thought to have self-assembled into lipid vesicles with intracellular chemical reactions. Eventually, these vesicles evolved in

complexity into protocells, with intracellular processes for energy conservation, synthesis of cell constituents, and a mechanism of self-replication[6,7]. These protocells were considered to have been primitive, largely devoid of complex intracellular processes. Unlike present-day cells, whose physiology, growth, and reproduction are regulated by complex molecular biological processes[8,9], such processes in protocells are thought to have been mediated by physicochemical properties of their cell constituents and fluctuating environmental conditions[7,10]. Despite being a key evolutionary link between abiotic chemical reactions on early Earth and prokaryotes, both the existence and mechanisms of their reproduction largely remained theoretical. Moreover, a mechanism of reproduction mediated entirely by physicochemical properties of cell constituents, leading to the formation of viable daughter cells has never been experimentally demonstrated. In the present study, we used a top-down approach to transforming a Gram-negative bacterium into a primitive protocell state and attempted to understand its mechanism of reproduction in its native habitat.

Our study differs from previous studies in two key aspects. First, rather than the conventional choice of using lipid vesicles (LVs), here we used protoplasts of the Gram-negative bacterium *Rhodobacter sphaeroides* (*RS-P*) as a proxy protocell. To date, most theoretical propositions on protocells were a result of studying lipid vesicles with the aqueous core as proxy protocells[7,11,12]. Despite accomplishing considerable progress in our theoretical understanding, we believe that studies conducted on LVs do not represent the true complexities of a self-replicating protocell. Even a primitive protocell should have possessed minimal biosynthetic pathways, a physiological mechanism of harvesting free energy from the surrounding (energy-yielding pathways), and a mechanism of replicating and transferring its genetic material to the daughter cells. The presence of these minimal physiological processes could incorporate considerable cytoplasmic complexity in a cell. Hence, we

consider bacterial protoplasts rather than LVs to be a more appropriate proxy for studying protocells. Moreover, protoplasts like the protocells, lack an innate ability to regulate their morphology or reproduction due to the loss of molecular biological coordination between intracellular processes[13,14].

Environmental conditions were proposed to have played an important role in facilitating protocell reproduction. Despite this proposition, most of the current studies were conducted under standard laboratory conditions. Hence, as the second novelty of our study, all our experiments were done under prebiotically plausible environmental conditions to understand the behavior of protocells in their native environment. The exact environmental conditions of early Earth are a matter of debate among researchers; Nevertheless, an emerging consensus among paleo-geologists suggests that surface temperatures of Archaean Earth (4000-2500 million years ago) ranged between 26° and 35°C[15,16], and the Archaean Eon oceans were 1.5 to 2 times saltier than the current oceans[17]. In support of this conclusion, all the earliest known signs of life like the Archaean Eon microfossils are restricted to coastal marine environment and are often found encrusted in salt[18,19]. This suggests protocells likely prevailed throughout the Archaean Eon in coastal marine environments and could have frequently experienced elevated salt concentrations. To replicate these conditions, we grew the bacterial protoplasts in media containing 7%Dead Sea salt (DSS) at 30°C. DSS was used in our incubations rather than pure NaCl to replicate the complex salt composition of Archaean oceans[20,21]. In the below sections of the manuscript, we present the lifecycle of these proxy-protocells in their native environment.

Results

The life cycle of proxy-protocells (*RS-P*) under Archaean Eon environmental conditions

We transformed the Gram-negative *Rhodobacter sphaeroides* (*DSM159*) into its protoplast state (*RS-P*) according to the procedure described in the methods section. Once we obtained stable protoplasts, we transferred them into fresh growth media containing 7%Dead Sea salt (DSS). We then monitored these cells at regular intervals using a variety of microscopic techniques. The lifecycle of these cells is shown in Fig. 1.

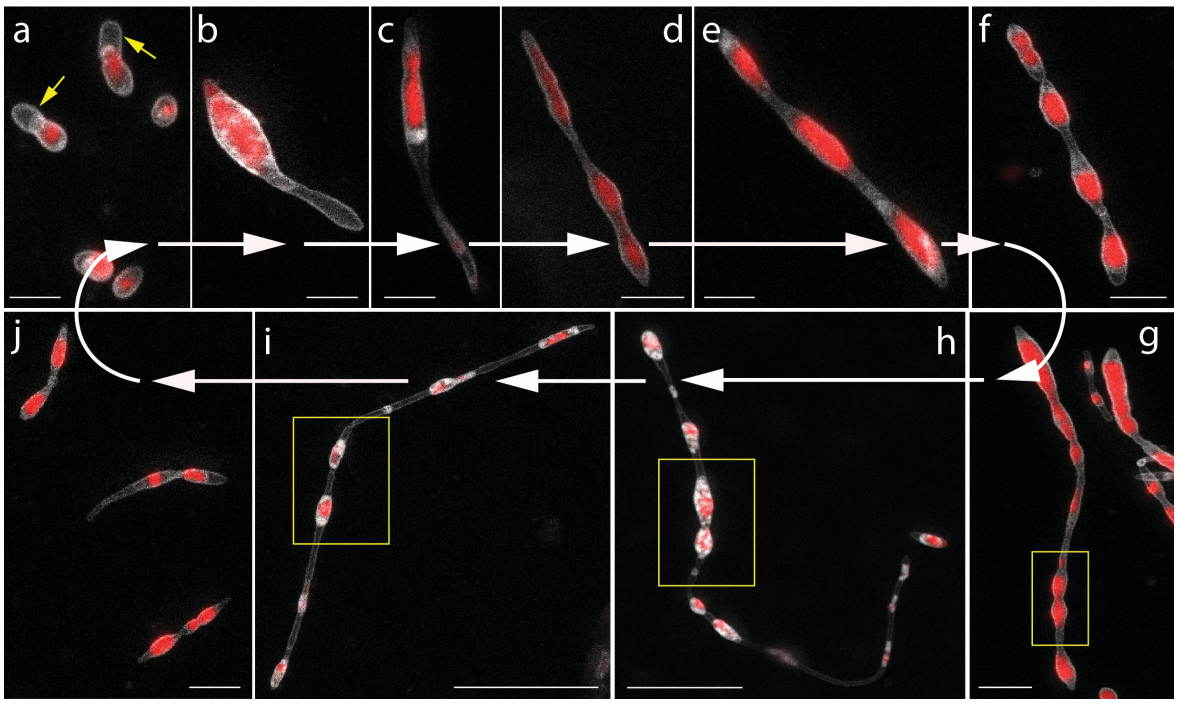

Fig. 1. The lifecycle of *RS-P*. All panels show STED microscopy images of cells stained with FM™5-95 (membrane, white) and PicoGreen™ (DNA, red). White arrows are a guide to the eye in following the life cycle progressing from **a** to **j**. Arrows (yellow) in **a** highlight cell with outer membrane extensions (are also seen in **b & c**). Transmission electron microscopy (TEM) images of such cells are shown in Supplementary Fig. 1. Boxed regions in **g-i** highlight cytoplasmic compartments within the filamentous cell undergoing binary fission. **j**: Individual cells with membrane overhangs formed from the fragmentation of filamentous cells. Scale bars: 2µm (**a-g** & **j**) and 10µm (**h** & **i**).

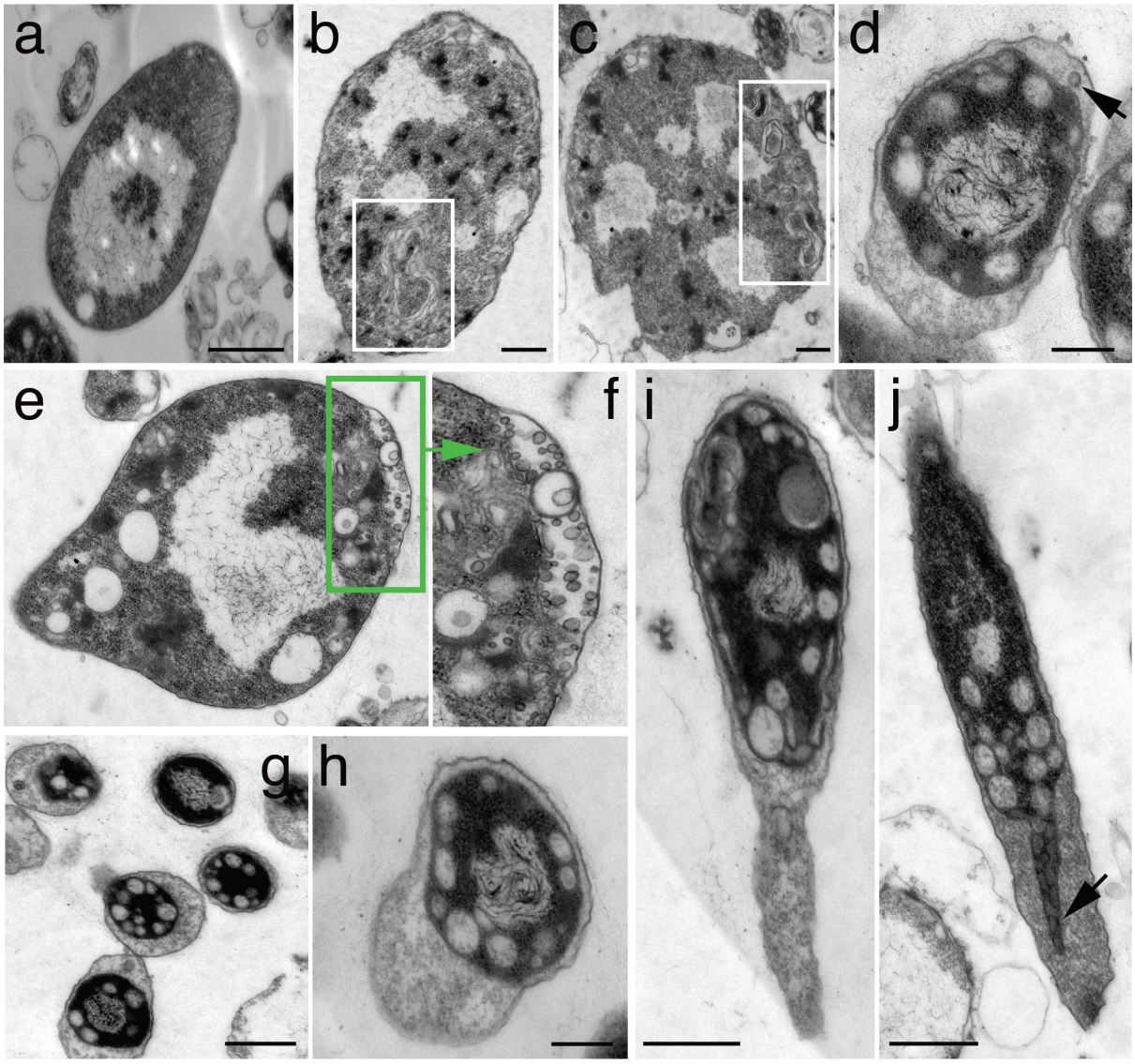

Fig. 2. TEM images of early growth stage *RS-P* cells. Images **a-c** show cells with folded excess membrane within the cell (highlighted regions). Image **d** show *RS-P* cells with intracellular vesicles. Arrow in **d** points to inner membrane undergoing budding into the periplasmic space. Image **e** show a cell with hollow membrane vesicles in the periplasmic space. Image **f** show the magnified periplasmic region of *RS-P* cell (in image **e**). Images **g-i** show cells with elongated outer membrane. Image **j** show growth of the cytoplasmic compartment filling in the void left by the outer membrane (arrow). Scale bars: 0.5µm (**a-j**).

During the lag phase, growth was restricted to the outer membrane of the cell, which expanded to form a hollow filamentous extension (Fig. 1a-c, Fig. 2 & Supplementary Fig. 1). The length of this tail varied from cell to cell, ranging between 0.5 to 5 μm (Fig. 1a-c, Fig. 2 & Supplementary Fig. 1). Most cells in this growth stage were observed to have developed hollow membrane vesicles, both within their cytoplasm and in the periplasmic space between the outer and the inner membranes (Fig. 2). These vesicles initially appeared as small buds attached to the inner cell membrane (Fig. 2d, arrow) followed by their expansion either into or out of the cytoplasm (Fig. 2d-f).

During the early-log phase, with an increase in the growth rate (Fig. 3), the volume of the cytoplasm increased, gradually filling the hollow template created by the outer membrane (Fig. 1c&d, 2j and Supplementary Fig. 1a-c). This led to the transformation of cells in sequence from spherical to tubular (Fig. 1&3 and Supplementary Fig. 1), then to dumbbell-shaped cells with cytoplasm mostly restricted to either end of the cell (Fig. 3, early log-phase). In the subsequent growth stages, cells developed surface depressions along their length resembling tubular vesicles subjected to curvature-induced destabilization at their surface (resembling Rayleigh-Plateau instability) (Fig. 1d-g, 3 & Supplementary Fig. 2). These surface depressions were formed as a result of the cytoplasmic compartment surrounded by the inner membrane undergoing binary fission (Fig. 1d-h & g-i).

Over time, these surface depressions grew deeper and two adjacent cytoplasmic compartments were linked to each other only by a hollow strand of outer membrane (boxed regions in Fig. 1h&i and Fig. 3 – late log phase). Rupture of the outer membrane connections led to the formation of individual daughter cells (Fig. 1j). This sequential transformation of cells was not observed when we repeatedly transferred log phase cells into fresh media every

few hours to keep cells in a prolonged log-phase. Cells in these experiments grew into longer and thicker filamentous cells without surface deformations (Supplementary Fig. 3). In the stationary growth phase (5-8 days from the start of the incubation), cell morphologies were a mix of all the above-described morphologies together with a considerable amount of membrane debris (Supplementary Fig. 4).

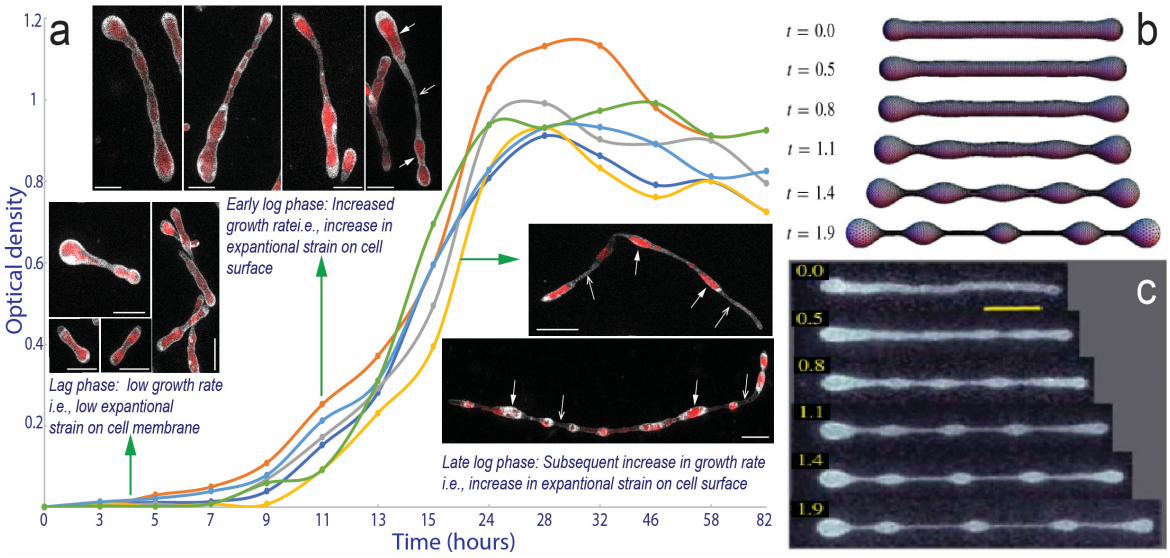

Fig. 3. *RS-P* cells in different growth stages and comparison of their morphology with LVs. Image **a** show the growth curve and morphologies of *RS-P* in different growth stages. Cells were stained, imaged, and color-coded as in Fig. 1. Closed and open arrows point to cytoplasmic compartments and to hollow outer membrane connecting the cytoplasmic compartments, respectively (also shown in Figures 4). Images **b** and **c** show theoretically predicted and experimentally observed morphologies of vesicles subjected to elongational stress over time (t) (images **b** & **c** were originally published by Narsimhan et al., 2015[22], reproduced here with permission from Cambridge University Press). Similar comparison of *RS-P* cells with LVs undergoing expansion are shown in Supplementary Fig. 2. Scale bar: 1μm (lag & early log-phase), 10μm (late log-phase).

Liquid-Liquid phase separation in cell membrane

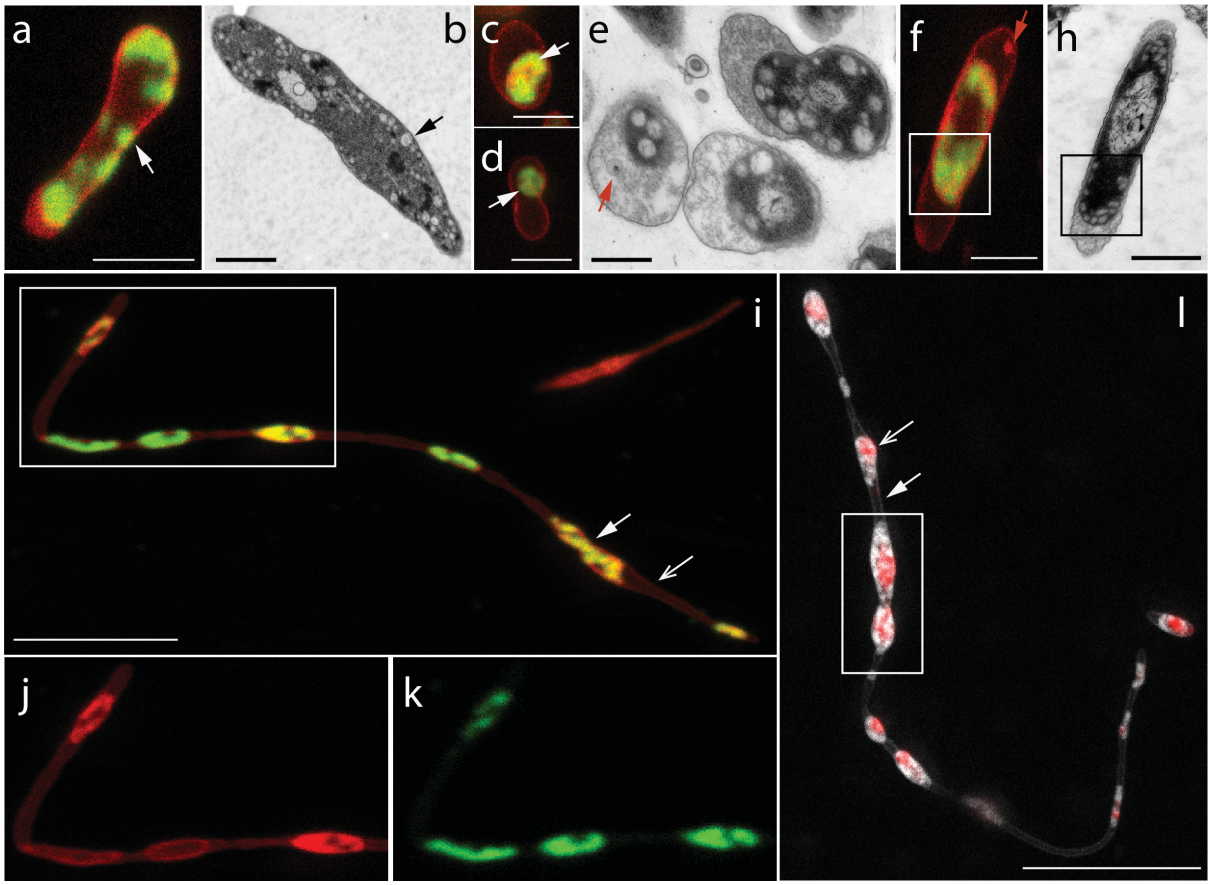

Fig. 4. Membrane phase separation in live *RS-P* cells. Cells in images **a**, **c**, **d**, **f**, **i**, **j**, & **k** are stained with FM™5-95 (all membrane, red) and *FAST*™ Dil (L_d-membrane, green). **a & b:** confocal and TEM images of early growth stage cell. Arrows in image **a** point to regions of the cell with L_d-membrane. Arrows in image **b**, points to similar intracellular vesicles. **c-h:** confocal and TEM images of later growth stage cells. Arrows in **c** & **d** are pointing to the cytoplasmic compartment, exclusively enclosed in L_d-membrane. Arrows (red) in **e**, points to the vesicles in periplasmic space (composed of Lo-membrane, red). Similar periplasmic vesicles can also be seen in Figure S1. **i**: Late log-phase filamentous *RS-P* cells (see Supplementary Fig. 5&6 for multiple optical sections of this stack). **j, k**: Magnified regions of the boxed region in **i** in individual channels. **l**: Filamentous *RS-P* cells stained as in Figure 1. Scale bars: 1µm (**a**, **c**, **d**, **f**,), 500nm (**b**, **e** & **h**) and 10µm (**i** & **l**).

Staining *RS-P* cells with both universal membrane dyes (FM™5-95) and a dye specific for the liquid-disordered phase (L_d) (*FAST*™Dil) showed the existence of two distinct phases within the cell membrane - liquid-ordered (L_o) and liquid-disordered (L_d) phases (Fig. 4 & Supplementary Fig. 5&6). During early growth stages, cell membrane underwent phase-separation and both L_d and L_o-membrane underwent invagination forming hollow buds. All the buds extending into the cytoplasm were exclusively composed of the L_d-membrane (Fig. 4a-e), and buds extending out of the cytoplasm into the periplasmic space were composed of the L_o-membrane (Fig. 4f, arrow). Over time we observed a gradual enrichment of more fluid L_d-phase within the inner cell membrane and more rigid L_o-phase within the outer cell membrane (Fig. 4 & Supplementary Fig. 5&6).

Influence of environmental conditions on *RS-P*'s morphology

To understand the influence of individual salts on the morphology of *RS-P*, we repeated the above experiments replacing DSS in the growth media with an equivalent concentration of divalent and monovalent salts like $MgCl_2$ or KCl/NaCl. Cells grown under these conditions exhibited morphologies similar to the cells grown in DSS (Fig. 5). However, considerable differences were observed in cell diameter – considerably thicker and longer filamentous cells (Fig. 5a-d) and considerably smaller individual cells (Fig. 5e-h) were observed when cells were grown in media containing 7%KCl and 7%$MgCl_2$ respectively. Thick tubular cells or long filamentous cells with diameter >1-2μm were rarely observed in incubations with $MgCl_2$, often only transiently during the log-phase (Fig. 5f&g).

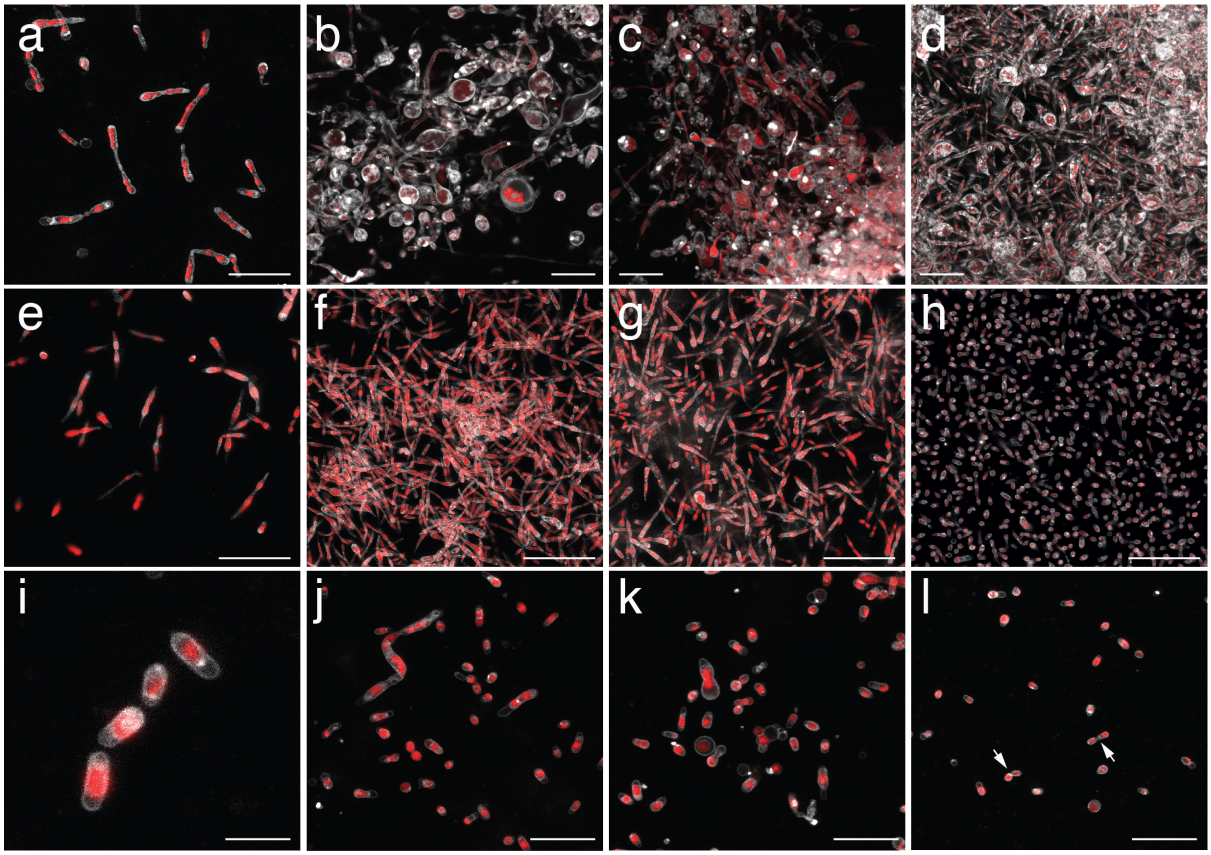

Fig. 5. Influence of salt composition on *RS-P*'s morphology

Images **a-d** show *RS-P* cells grown in 7%DSS-NB from early to late growth stages. Images **e-h** show *RS-P* cells grown in 7%DSS-NB from early to late growth stages. Images **i-l** show *RS-P* cells grown in 7%DSS-NB from early to late growth stages. Arrows in image **i** points to cells undergoing binary fission. Cells were stained, imaged, and color-coded as in Fig. 1. Scale bars (10 μm).

Efficiency of *RS-P*'s reproductive process

The concentration of extracellular DNA was used as a proxy to determine the leakage of intracellular constituents during reproduction. Results of this quantification was presented in Fig. 5. Quantifiable but no significant differences in the concentration of extracellular DNA was observed between *RS-P* and the native *R. spheroides* cells which possess a well-

functioning molecular biological regulatory process (Fig. 6a). Neither were significant differences observed between cells grown in media containing different salts. The reproductive efficiency was marginally higher when *RS-P* was incubated on an orbital shaker rather than under static conditions (Fig. 6b). Staining and imaging of the stationary growth phase incubations also suggest the absence of extracellular DNA.

The metabolic viability of *RS-P* daughter cells was determined by staining daughter cells from the stationary growth phase with stains specific for DNA and cytoplasmic activity. Quantification of live cells was done by flow cytometry. Our results suggest, most of the daughter cells (< 70%) received DNA from the parent cell and are physiologically active (< 80%) with intracellular enzyme activity (Fig. 6e). Subsequent transfer of daughter cells of different ages – 10, 20, 100day old cultures into a fresh media always resulted in growth.

Discussion

The above-described life cycle of *RS-P* could be explained by the biophysical properties of its cell constituents together with a lack of molecular biological coordination between physiological processes within the cell. This loss of coordination leading to chaotic behavior of cells[13,14,23] together with excessive lipids synthesis[24] was previously reported in protoplasts. In accordance with these studies, cells in our study were observed to be in a perpetual state of lipids excess (Fig. 2). This is evident by the presence of excessive membrane observed within *RS-P* during all growth stages (Supplementary Fig.1c&d and Fig. 2). Morphological features observed in *RS-P* like the outer membrane extensions, hollow vesicles within the cells, and transformation of tubular cells to a string-of-beads morphology (Fig. 3) can be explained as a mechanism of accommodating excess cell membrane. Transfer

of lipids synthesized within the cytoplasm to the outer membrane and its subsequent expansion into a filamentous structure happened by a two-step process. In the first step, disproportionately high lipid synthesis in comparison to cytoplasmic volume increase (low growth rate during lag-phase) facilitated the transformation of the excess membrane into a bud (Fig. 2d-f). Subsequently, these hollow buds detached from the inner membrane and were released into the periplasmic space (Fig. 2e-f). In step two, these hollow vesicles fused and incorporated into the outer membrane, leading to its expansion (Fig. 1b & Fig. 2d-j).

Membrane phase separation and subsequent budding can be explained by the model proposed by Lipowsky & Jülicher[25,26]. It was hypothesized that when membranes undergo liquid-liquid phase-separation, more fluid L_d-membrane spontaneously undergo out-of-plane invagination, transforming into a bud to reduce line tension at the phase-boundary[27]. The transformation of L_d-membrane into intracellular vesicles (Fig. 4) is in tune with this hypothesis. Nevertheless, apart from more fluid L_d-membrane we also observed L_o-membrane with high bending rigidity and low spontaneous curvature undergoing budding (Fig. 4f). The formation of these structures can be explained by the chemical composition of the cell membrane[28]. Recent studies attempting to understand complex cell membranes demonstrated the possibility of L_o-membranes forming buds. Apart from the thermodynamic considerations, presence of certain sterols in the membrane is shown to induce invagination and subsequent budding of L_o-membrane[28]. In accordance with these studies, Gram-negative bacteria like *RS-P* and in particular, anoxic phototrophs were known to have a diverse sterols composition in their plasma membrane[29], which could have played a role in the budding of L_o-membranes.

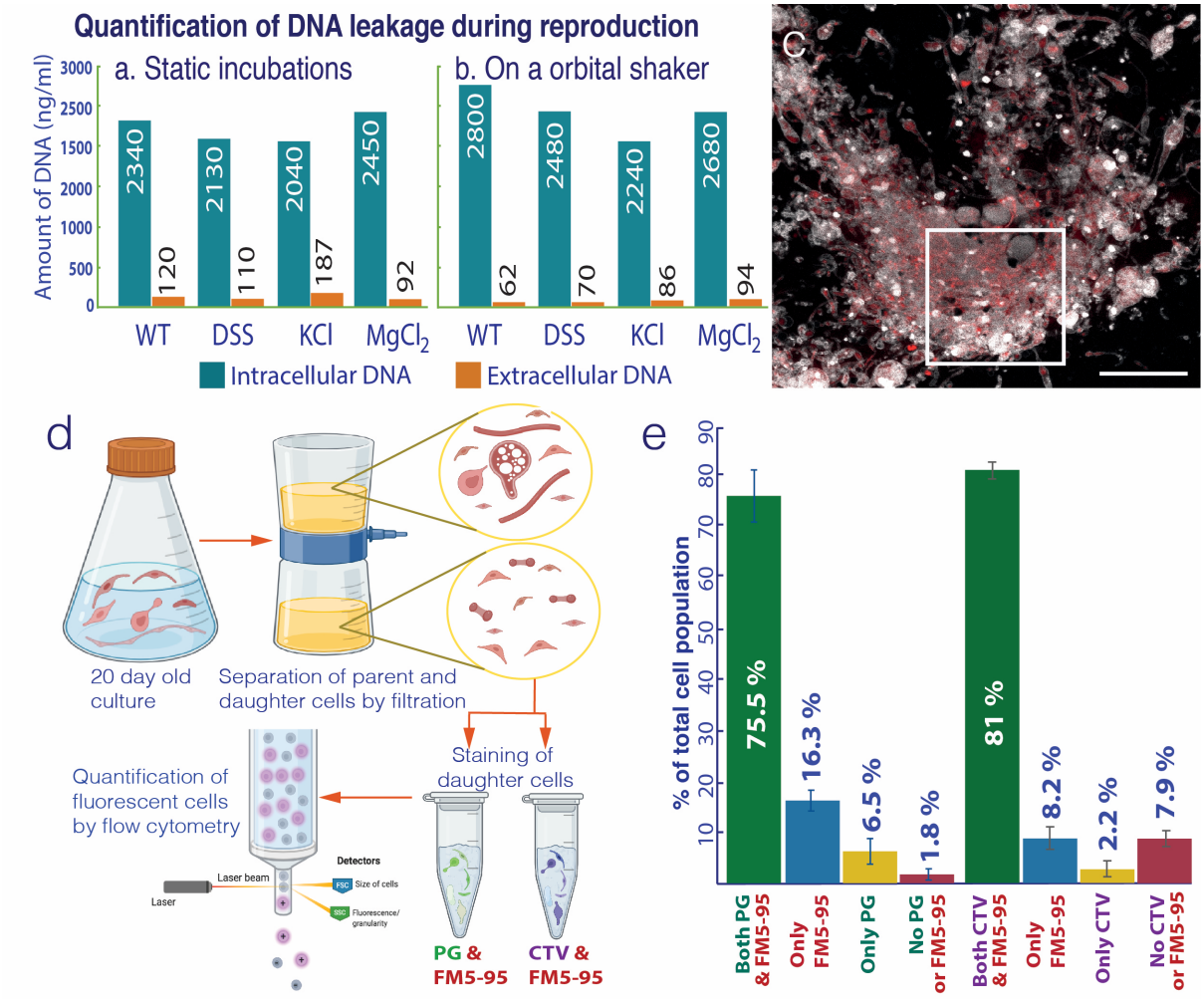

Fig. 6. Reproductive efficiency and viability of *RS-P* daughter cells. Graphs **a** & **b** show intracellular (blue bars) and extracellular (orange bars) DNA concentrations (n=5 for each condition). **a:** *RS-P* grown under static conditions. **b:** *RS-P* grown on an orbital shaker. Annotations: WT (wild type, *R. sphaeroides* with a cell wall grown in NB); DSS, KCl & $MgCl_2$ – *RS-P* grown in NB with respective salts. Image c show *RS-P* cells in late growth stage. Cells in this image are stained as described in Figure 1. **d**: Schematic workflow of the experiment to determine the live daughter cells. **e**: Percentage of *RS-P* daughter cells that were identified positive for different viability markers in flow cytometry. Cells were stained with different combinations of FM™5-95 (cell membrane), PicoGreen™ (PG, DNA), and CellTrace™ Violet (CTV, cell integrity) (n=3, in the plot but multiple repetitions over the

course of the work). The original flow cytometry plots together with the confocal microscope images of daughter cells are shown in Supplementary Fig. 7&8.

The nature and direction of the membrane invagination could also have been determined by differences in the osmolarities and packing densities differences within the cytoplasm[30]. L_d and L_o-membranes were previously shown to selectively associate with regions of higher and lower densities. This phenomenon could explain the preferential association of L_d-membrane with the cytoplasm (~17-35 wt% molecules), always forming vesicles into the cell and L_o-membrane preferentially invaginating out of the cell into the surrounding media (~6-7 wt% molecules). Differences in the packing densities between the cytoplasm and the periplasmic space or the surroundings can also be inferred from the TEM images (Supplementary Fig. 1)[31].

Lipid raft hypothesis and the existence of Liquid-Liquid phase separation in live cells was first proposed in 1997[32]. Nevertheless, the existence of such distinct phases in live cells has been a point of contention among researchers[33]. Decades of back-and-forth arguments led to the consensus, that the only way of conclusively resolving this issue is to provide visual evidence of membrane phase separation in a live cell[33]. To the best of our knowledge, ours is the first study to provide such direct evidence (Fig. 4). However, given the loss of molecular biological regulatory processes within the cell, we propose the membrane phase-separation we observed was a passive thermodynamic phase-separation rather than a functional membrane phase-separation linked to a certain cellular function or mediated by the intracellular processes[32].

Morphologies of *RS-P* observed during subsequent growth stages can be explained solely from a physicochemical perspective. Growth (or expansion) of the cytoplasmic compartment

within the cell, gradually filling the void left by the outer membrane resembles LVs undergoing stretching when placed in an elongational flow path (Fig. 2 & Supplementary Fig. 2)[22]. Like the LVs, morphologies of *RS-P* can be explained by the physical properties of the cell membrane like its elasticity and expansion strain exerted on the membrane[22,34] due to cytoplasmic volume increase. Spherical LVs experiencing a low elongational strain were shown to transform into prolate or tubular shapes[34] (Fig. 3b&c and Supplementary Fig. 2). However, at a certain strain level (threshold strain), vesicles transformed into a dumbbell shape. Upon further strain increase, vesicles formed elongated dumbbells with beaded structures appearing along its length. *RS-P* exhibited a similar pattern of morphological transformation (Fig. 3 & Supplementary Fig. 2). In the case of *RS-P*, high and low elongational strains on the membrane translate into high and low growth rates (i.e., rate of cytoplasmic volume increase). In accordance with this hypothesis, short prolate or tubular cells were most frequently observed during an early lag-phase, when the growth rate of the cell was low compared to other growth stages (Fig. 3). With an increase in their growth rate during the mid/late-log phase, *RS-P* transformed into elongated dumbbells and subsequently into dumbbell-shaped cells with beaded structures along their length (Fig. 3). The subsequent reduction in the growth rate due to the depletion of nutrients in the growth media (stationary phase), which transformed *RS-P* into string-of-beads morphology (Fig.1h&i and Fig. 3). These results suggest that growth rate played an important role in determining cell morphology. In support of this conclusion, cells kept in a prolonged log-phase gradually increased both in length and diameter without transformation into a string-of-beads morphology (Supplementary Fig. 3).

Together with the elongational strain, the morphological transformation of *RS-P* can also be explained from a thermodynamic perspective as proposed by Area differential elasticity

(ADE) theory[35,36]. According to ADE theory morphology of LVs or in the present study *RS-P,* is largely determined by the ratio of the area of the cell membrane to its cell volume. When LVs are placed in hyperosmotic solution, they undergo osmotic deflation[37] accompanied by a change in their morphology to attain a thermodynamically stable state. Given the inherent excess membrane synthesis in *RS-P*, cells in our study were observed to be in a perpetual state of membrane excess (Fig. 2). However, cell membrane area: volume is also determined by the growth rate (Fig. 3). The slow growth rate during the lag-phase resulted in the formation of outer membrane extensions. During the early and mid-log phases, a high rate of cytoplasmic volume (growth rate) increase keeps pace with membrane synthesis. This absence of excess membrane likely resulted in tubular cells with smooth surfaces (Fig. 3a). A gradual decrease in the growth rate by the end of the log-phase reverted cells to a state of excess membrane. Such a state could have caused the cells transformation into a string-of-beads morphology (Fig. 1h&i and Fig. 2a), to accommodate the excess membrane within the membrane tethers connecting the cytoplasmic compartments. In accordance with these interpretations, cells kept in a prolonged log-phase (high growth rate) grew into thicker and longer filaments without surface deformations (Supplementary Fig. 3).

Morphological differences between cells grown under different salt conditions (Fig. 5) can be explained by the nature of the interaction between phospholipid membranes and different cations[38]. It was reported that divalent cations like Mg^{+2} organize lipids into clusters of 10-15 molecules each[39], dehydrating and stiffening the membrane, thus hindering its area expansion. On the other hand, monovalent cations like K^{+} reduce the bending rigidity of the membrane, making the membrane more flexible[40] and conducive to the formation of larger cells. The absence of filamentous cells when *RS-P* was grown on a shaker (Fig. 5i-l) likely was due to the constant shearing of long filamentous cells. The reversible shift in the cell

morphology, when transferred between different incubations suggests that morphology is determined by the environmental conditions rather than the information encoded in its genome.

Earlier studies proposed that fission of protocells into daughter cells should have been achieved through physical forces[7,41]. Hence to achieve protocell fission (cell-division), these studies employed methods like extrusion through a narrow pore size filter or by application of external force[7,11,41]. As most cells in the last growth stage are primarily unicellular daughter cells formed by the fission of filamentous *RS-P* and given the fact that our experiments were conducted under static conditions, we do not assume cells-division in *RS-P* was a result of an external stimulus. We rather propose that the force required to mediate fission was intrinsic to the cell. Recent studies showed that the presence of an internal metabolism or Brownian movement of intracellular constituents[42,43] could result in surface instabilities leading to cell division[43,44]. In support of this presumption, cells in our incubations were intrinsically unstable (Movie S1, early growth phase cells with expanded outer membrane). They were in a constant state of oscillation, which should have been a result of Brownian movement of intracellular constituents[42,45] (Movie S1 & movement of DNA in spherical *RS-P* cells in the top half of Movie S2). This constant movement of intracellular constituents could have led to the generation of force required for the fission of daughter cells in *RS-P*[43]. In support of this presumption, we observed cells within a filament were in a constant pull-and-push motion, which ultimately could have resulted in cell fission (Movie S3-S5). The absence of intracellular content leakage suggests that loss of molecular biological coordination didn't considerably affect the reproductive efficiency (Fig. 6). However, the presence of a considerable amount of membrane debris (Supplementary Fig. 4) and large clumps of cells were observed in the stationary growth phase (Fig. 6c). These clumps could have formed by

the entanglement of filamentous cells (Supplementary Fig. 9). Observation of these clumps at regular intervals after their formation showed no evidence for the formation of individual daughter cells. Moreover, most such clumps were consisted of disintegrated cells leading to the formation of cell debris (Supplementary Fig. 9). These observations suggest that *RS-P* reproduced less efficiently than the cells in its original cell state. However, given the absence of long filamentous cells and large cell clumps when grown on an orbital shaker (Fig. 5i-l and Fig. 6e), we presume such cells reproduced more efficiently under turbulent natural environments rather than in our static incubations.

Processes like growth and reproduction are punctiliously regulated by the timely expression of certain genes and precise localization of proteins within the cell[46]. This thigh coordination between anabolic processes, growth, and reproduction is considered essential for the proper functioning of the cell[47]. In contrast to this current understanding, here we demonstrated not only that cells can reproduce when they lose their molecular biological coordination, but such a lack of coordination is necessary for efficient reproduction under the environmental conditions of early Earth. Most *RS-P*'s morphologies and formation of daughter cells can be attributed to this loss of intracellular regulation and the resulting imbalance between the area of the cell membrane to its volume. The efficiency with which these cells reproduced can only be explained by the multilamellar nature of the cell membrane and by the formation of long filamentous cells by the sequential expansion of outer followed by inner cell membrane[7]. Thereby preventing the leakage of intracellular constituents.

The mechanism of reproduction we described above is in accordance with the theoretical propositions on protocells[7]. However, no direct proof exists to conclusively state that protocells inhibiting early Earth did in fact reproduced by this process. To verify the validity

of our proposition that protocells reproduced by these processes, we compared very distinctive *RS-P* morphologies observed in our study with the oldest known microfossils from 3.8-billion-year-old rock formations[48]. An extensive comparison of the cell morphologies, and elemental and isotopic composition of these microfossils is beyond the scope of the current study and is presented as an accompanying manuscript[48]. The result of this study provides independent proof for the existence of cells reproducing by this process on early Earth.

In the present study, we demonstrated a method of reproduction, driven entirely by physicochemical processes. Favorable environmental conditions and lack of coordination between different physiological processes within the cell are key/primary drivers of this method of reproduction. Given the simplicity and efficiency with which these cells reproduced under environmental conditions of early Earth, we propose protocells likely reproduced by a similar process. Our study also establishes protoplasts as a better experimental model organisms to study protocells.

Methods and Materials

Gram-negative bacteria and its cultivation

Gram-negative *Rhodobacter sphaeroides* (*DSM159*) was obtained from DMSZ (Braunschweig, Germany). Lyophilised cells were revived in nutrient broth (Sigma Aldrich, Germany) according to the procedure described by DSMZ.

Generation of bacterial protoplasts

Protoplasts were generated from *R. sphaeroides* (*RS-P*) by inoculating overnight cultures into three times concentrated nutrient broth (NB) containing, 1% w/v sucrose, 80 µg/ml Lysozyme and 200µg/ml Penicillin G (Sigma Aldrich, Germany). Transformation to their protoplast state was confirmed by observing the cell under a microscope. Over the next 3-4 weeks the cells were repeatedly sub-cultured into fresh media with penicillin G and lysozyme as described above. Subsequently *RS-P* was transferred into NB with 7% Dead Sea Salt (DSS) (Amazon.de). Stability of these protoplasts (*RS-P*) was determined after ten sub-cultures by transferring cells into media without Penicillin G or Lysozyme. As *RS-P* did not revert to its native state with cell wall under these conditions, Lysozyme and Penicillin G was not added to the growth media for subsequent experiments. Unless otherwise stated, cells in the rest of the experiments were grown in 7%DSS-NB. In some experiments, we replaced DSS in the growth media with equivalent concentrations of other salts like $MgCl_2$ and KCl (7%w/v).

Quantification of bacterial growth

RS-P was grown under conditions described above and growth was quantified at intervals shown in Figure 2 using an Biophotometer® D30 (Eppendorf, Germany).

Phase-contrast and Super-resolution STED microscopy

Morphology *RS-P* was determined at regular intervals using a Axioskop 2plus microscope (Carl Zeiss, Germany) using a Plan-NEOFLUAR 100X/1.3 objective. Images were acquired with Leica DSF9000 (Leica, Germany) cameras. STED microscopy was performed with an inverted TCS SP8 STED 3X microscope (Leica Microsystems, Mannheim Germany) using

an 86x/1.2 NA water immersion objective (Leica HC PL APO CS2 - STED White). Fluorophores were excited with either 488, 561nm, 594nm or 633m laser light derived from 80 MHz pulsed White Light Laser (Leica Microsystems, Mannheim Germany). For stimulated emission, either a pulsed 775 nm laser or a 592nm CW laser (Leica Microsystems, Mannheim Germany) was used depended on the fluorophore. The emitted fluorescence light was collected with Hybrid Detectors (HyD, Leica Microsystems, Mannheim Germany) using appropriate emission band pass-filter setting and typically a gate of 0.3ns-6.0ns for depletion with the 775nm laser or 1.0-6.0ns with the 592nm laser. Images were recorded in photon counting mode and line accumulation. Image deconvolution was performed on selected images and movies with Huygens Professional (version 16.10.1p2, Scientific Volume Imaging, Hilversum, The Netherlands).

Transmission electron microscopy

RS-P cells at different growth stages were harvested from the growth media by centrifugation at 500rpm for 5min. Cells were then preserved in 2.5% v/v glutaraldehyde (Carl Roth, Karlsruhe, Germany). Cells were subsequently stained with 0.25% w/v uranyl acetate. Cells were subsequently dehydrated in increasing concentration of acetone. Cells were embedded in epoxy resin and left for polymerisation for 72h. Epoxy blocks were then sectioned, and cells were counter stained with 1% lead citrate. TEM was carried out using a Zeiss EM 912 (Zeiss, Oberkochen) with an integrated OMEGA-filter at 80kV. Images were acquired with 2k x 2k pixel slow scan CCD camera (TRS, TrÖndle Restlichtverstrkersysteme, Moorenweis, Germany) and an ImageSP software (version 1.2.9.77) (SysProg, Minsk, Belarus).

Quantifying reproductive efficiency and metabolic viability of daughter cells

Reproductive efficiency was determining the leakage of cell constituents during the formation of daughter cells. Viability of daughter cell was determined by staining and quantifying cells by flow cytometry.

RS-P was inoculated into nutrient broth containing 7% w/v of DSS, NaCl and $MgCl_2$. The culture bottles were either incubated under static conditions or on an orbital shaker at 160 rpm. 2ml of cells were harvested every 24h time intervals from all the incubations. In case of static cultures, incubations were briefly placed on an orbital shaker for 10 min at 100 rpm to disperse the biofilm. Intact cells were precipitated by centrifugation at 6000 rpm for 10 min. DNA was extracted from both cell and supernatant. In the final step, DNA was washed with 70% ethanol for three times to remove any residual salts from DNA. The resultant DNA was dissolved in 2ml of TE buffer. Quantification of DNA was done using Qubit dsDNA quantification kit (Invitrogen). All the experiments were done in replicates (n=5).

Viability of daughter cells was determined by growth of daughter cells either by directly sub-culturing 10-20 day old cultures into fresh media or by passing 10-20 day old cultures through 0.45µm cellulose acetate filter (Millipore) and then transferring the filtrate into fresh media. Presence of DNA and cytoplasmic activity of daughter cells was also tested by staining them with DNA stain, PicoGreen™ (Invitrogen) and live cell stain CellTrace™ violet stain (Invitrogen). Cells with intracellular DNA and cytoplasmic activity were quantified using flowcytometry (Attune NxT, Thermo Fisher scientific).

References

1. Oparin, A. I. Chemistry and the origin of life. *R. Inst. Chem. Rev.* (1969). doi:10.1039/rr9690200001
2. Miller, S. L. A production of amino acids under possible primitive earth conditions. *Science (80-.).* **117**, 528–529 (1953).
3. Mariani, A., Russell, D. A., Javelle, T. & Sutherland, J. D. A Light-Releasable Potentially Prebiotic Nucleotide Activating Agent. *J. Am. Chem. Soc.* **140**, (2018).
4. Powner, M. W., Gerland, B. & Sutherland, J. D. Synthesis of activated pyrimidine ribonucleotides in prebiotically plausible conditions. *Nature* **459**, (2009).
5. Rajamani, S. *et al.* Effect of stalling after mismatches on the error catastrophe in nonenzymatic nucleic acid replication. *J. Am. Chem. Soc.* **132**, (2010).
6. Chen, I. A., Salehi-Ashtiani, K. & Szostak, J. W. RNA catalysis in model protocell vesicles. *J. Am. Chem. Soc.* **127**, 13213–13219 (2005).
7. Zhu, T. F. & Szostak, J. W. Coupled growth and division of model protocell membranes. *J. Am. Chem. Soc.* **131**, 5705 (2009).
8. Navarro, P. P. *et al.* Cell wall synthesis and remodelling dynamics determine division site architecture and cell shape in Escherichia coli. *Nat. Microbiol.* **7**, 1621–1634 (2022).
9. Eswara, P. J. & Ramamurthi, K. S. Bacterial Cell Division: Nonmodels Poised to Take the Spotlight. *Annual Review of Microbiology* **71**, (2017).
10. Kudella, P. W. *et al.* Fission of Lipid-Vesicles by Membrane Phase Transitions in Thermal Convection. *Sci. Rep.* **9**, (2019).
11. Hanczyc, M. M., Fujikawa, S. M. & Szostak, J. W. Experimental models of primitive cellular compartments: encapsulation, growth, and division. *Science (80-.).* **302**, 618–

622 (2003).

12. Budin, I. & Szostak, J. W. Physical effects underlying the transition from primitive to modern cell membranes. *Proc. Natl. Acad. Sci.* **108**, 5249–5254 (2011).

13. Wu, L. J. *et al.* Geometric principles underlying the proliferation of a model cell system. *Nat. Commun.* **11**, (2020).

14. Leaver, M., Dominguez-Cuevas, P., Coxhead, J. M., Daniel, R. A. & Errington, J. Life without a wall or division machine in Bacillus subtilis. *Nature* **457**, 849 (2009).

15. Blake, R. E., Chang, S. J. & Lepland, A. Phosphate oxygen isotopic evidence for a temperate and biologically active Archaean ocean. *Nature* **464**, (2010).

16. Catling, D. C. & Zahnle, K. J. The Archean atmosphere. *Sci. Adv.* **6**, (2020).

17. Knauth, L. P. Salinity history of the Earth's early ocean. *Nature* **395**, 554 (1998).

18. Alleon, J. *et al.* Chemical nature of the 3.4 Ga Strelley Pool microfossils. *Geochemical Perspect. Lett.* **7**, 37–42 (2018).

19. Walsh, M. W. Microfossils and possible microfossils from the early archean onverwacht group, barberton mountain land, South Africa. *Precambrian Res.* **54**, 271–293 (1992).

20. Moore, E. K., Jelen, B. I., Giovannelli, D., Raanan, H. & Falkowski, P. G. Metal availability and the expanding network of microbial metabolisms in the Archaean eon. *Nature Geoscience* **10**, (2017).

21. Johnson, T. E., Brown, M., Kaus, B. J. P. & Vantongeren, J. A. Delamination and recycling of archaean crust caused by gravitational instabilities. *Nat. Geosci.* **7**, (2014).

22. Narsimhan, V., Spann, A. P. & Shaqfeh, E. S. G. Pearling, wrinkling, and buckling of vesicles in elongational flows. *J. Fluid Mech.* (2015). doi:10.1017/jfm.2015.345

23. Kawai, Y. *et al.* Cell growth of wall-free L-form bacteria is limited by oxidative damage. *Curr. Biol.* **25**, 1613–1618 (2015).

24. Mercier, R., Kawai, Y. & Errington, J. Excess membrane synthesis drives a primitive mode of cell proliferation. *Cell* **152**, 997–1007 (2013).

25. Lipowsky, R. Budding of membranes induced by intramembrane domains. *J. Phys. II* (1992). doi:10.1051/jp2:1992238

26. Jülicher, F. & Lipowsky, R. Domain-induced budding of vesicles. *Phys. Rev. Lett.* (1993). doi:10.1103/PhysRevLett.70.2964

27. Baumgart, T., Hess, S. T. & Webb, W. W. Imaging coexisting fluid domains in biomembrane models coupling curvature and line tension. *Nature* (2003). doi:10.1038/nature02013

28. Bacia, K., Schwille, P. & Kurzchalia, T. Sterol structure determines the separation of phases and the curvature of the liquid-ordered phase in model membranes. *Proc. Natl. Acad. Sci. U. S. A.* (2005). doi:10.1073/pnas.0408215102

29. Rashby, S. E., Sessions, A. L., Summons, R. E. & Newman, D. K. Biosynthesis of 2-methylbacteriohopanepolyols by an anoxygenic phototroph. *Proc. Natl. Acad. Sci.* **104**, 15099–15104 (2007).

30. Andes-Koback, M. & Keating, C. D. Complete budding and asymmetric division of primitive model cells to produce daughter vesicles with different interior and membrane compositions. *J. Am. Chem. Soc.* **133**, (2011).

31. Sandoz, P. A., Tremblay, C., Gisou van der Goot, F. & Frechin, M. Image-based analysis of living mammalian cells using label-free 3D refractive index maps reveals new organelle dynamics and dry mass flux. *PLoS Biol.* **17**, (2019).

32. Simons, K. & Ikonen, E. Functional rafts in cell membranes. *Nature* (1997). doi:10.1038/42408

33. Sezgin, E., Levental, I., Mayor, S. & Eggeling, C. The mystery of membrane organization: Composition, regulation and roles of lipid rafts. *Nature Reviews*

Molecular Cell Biology (2017). doi:10.1038/nrm.2017.16

34. Kantsler, V., Segre, E. & Steinberg, V. Critical dynamics of vesicle stretching transition in elongational flow. *Phys. Rev. Lett.* (2008). doi:10.1103/PhysRevLett.101.048101

35. Yanagisawa, M., Imai, M. & Taniguchi, T. Periodic modulation of tubular vesicles induced by phase separation. *Phys. Rev. E - Stat. Nonlinear, Soft Matter Phys.* (2010). doi:10.1103/PhysRevE.82.051928

36. Yanagisawa, M., Imai, M. & Taniguchi, T. Shape deformation of ternary vesicles coupled with phase separation. *Phys. Rev. Lett.* (2008). doi:10.1103/PhysRevLett.100.148102

37. Sanborn, J., Oglęcka, K., Kraut, R. S. & Parikh, A. N. Transient pearling and vesiculation of membrane tubes under osmotic gradients. *Faraday Discuss.* (2012). doi:10.1039/c2fd20116j

38. Tsai, H. H. G. *et al.* Molecular dynamics simulation of cation-phospholipid clustering in phospholipid bilayers: Possible role in stalk formation during membrane fusion. *Biochim. Biophys. Acta - Biomembr.* **1818**, (2012).

39. Schultz, Z. D., Pazos, I. M., McNeil-Watson, F. K., Lewis, E. N. & Levin, I. W. Magnesium-induced lipid bilayer microdomain reorganizations: Implications for membrane fusion. *J. Phys. Chem. B* (2009). doi:10.1021/jp9011944

40. Karimi, M. *et al.* Asymmetric Ionic Conditions Generate Large Membrane Curvatures. *Nano Lett.* (2018). doi:10.1021/acs.nanolett.8b03584

41. Deshpande, S., Spoelstra, W. K., Van Doorn, M., Kerssemakers, J. & Dekker, C. Mechanical Division of Cell-Sized Liposomes. *ACS Nano* **12**, (2018).

42. Di Rienzo, C., Piazza, V., Gratton, E., Beltram, F. & Cardarelli, F. Probing short-range protein Brownian motion in the cytoplasm of living cells. *Nat. Commun.* **5**, (2014).

43. Fisher, J. K. *et al.* Four-dimensional imaging of E. coli nucleoid organization and dynamics in living cells. *Cell* **153**, (2013).

44. Zwicker, D., Seyboldt, R., Weber, C. A., Hyman, A. A. & Jülicher, F. Growth and division of active droplets provides a model for protocells. *Nat. Phys.* (2017). doi:10.1038/nphys3984

45. Vutukuri, H. R. *et al.* Active particles induce large shape deformations in giant lipid vesicles. *Nature* **586**, (2020).

46. Khanna, K., Lopez-Garrido, J., Sugie, J., Pogliano, K. & Villa, E. Asymmetric localization of the cell division machinery during bacillus subtilis sporulation. *Elife* **10**, (2021).

47. Lozada-Chávez, I., Janga, S. C. & Collado-Vides, J. Bacterial regulatory networks are extremely flexible in evolution. *Nucleic Acids Res.* **34**, (2006).

48. Kanaparthi, D. *et al.* On the nature of the earliest known lifeforms. *bioRxiv* 2021.08.16.456462 (2021). doi:10.1101/2021.08.16.456462

Acknowledgments

We would like to thank Petra Schwille for her support and scientific input throughout the work and in preparing the manuscript, Gabriella Berthal and Markus Oster for excellent technical support. We thank the Advanced Light Microscopy Facility at EMBL, Heidelberg, Ulf Schwartz from Leica Microsystems, colleagues at the departments of Ecological Microbiology (Bayreuth University) and of Cellular and Molecular Biophysics (Max Planck Institute for Biochemistry) for their support throughout the work.

Funding

This research was funded by the European Research Council (ERC) grant agreement 616644 (POLLOX), and by the Deutsche Forschungsgemeinschaft (DFG) grant agreements DFG-TRR174 and Seed funding from Excellence Cluster ORIGINS EXC2094 – 390783311.

Author contributions

Conceptualization: DK, ML, BZ & TL. Culture experiments: DK. Electron microscopy: DK & AK. Light microscopy: DK & ML. Analysis: DK & JHK. Manuscript Writing: DK & JHK Manuscript Proof-reading: All authors.

Competing interests

The authors declare that they have no competing interests.

Data and materials availability

All source data associated with the study is available from the authors upon request.

Supplementary information

Supplementary Figures. 1 – 9 & Supplementary Movies. 1 – 4.